First-principles investigation of hydrogen trapping and diffusion at grain boundaries in nickel

Davide Di Stefano[a], Matous Mrovec[a], Christian Elsässer[a]

[a] *Fraunhofer-Institut für Werkstoffmechanik IWM, Wöhlerstr. 11, 79108 Freiburg, Germany*

Abstract

In this work, the interaction of hydrogen with high-angle GBs in nickel has been investigated by means of density functional theory simulations. Two distinct types of GBs have been considered: the $\Sigma3(111)[\bar{1}10]$ with a close-packed interface structure and the $\Sigma5(210)[001]$ with a less dense interface structure consisting of open structural units. Our calculations reveal that these two GBs have a markedly different interaction behavior with atomic hydrogen. The close-packed $\Sigma3$ GB neither traps H nor enhances its diffusion, but instead acts as a two-dimensional diffusion barrier. In contrast, the $\Sigma5$ GB provides numerous trapping sites for H within the open structural units as well as easy migration pathways for H diffusion along the GB plane that can enhance the H diffusivity by about two orders of magnitude compared to bulk Ni. The obtained results are analysed in detail and compared with available experimental and other theoretical data.

Keywords: Hydrogen embrittlement, nickel, grain boundary, diffusion, segregation

1. Introduction

Hydrogen is known to have a deleterious effect on mechanical properties of many metals and alloys. This phenomenon, known as hydrogen embrittlement (HE), has been studied intensively over decades but its underlying microscopic mechanisms are still debated and not fully understood (for reviews see [1, 2, 3, 4, 5, 6]). For structural materials, which do not form hydrides, such as Ni, several mechanisms responsible for HE have been proposed including hydrogen enhanced decohesion (HEDE), hydrogen enhanced local plasticity (HELP), adsorption-induced dislocation emission, or hydrogen enhanced strain induced vacancy formation. Although all these mechanisms are of different nature, they are not mutually exclusive and are likely to occur simultaneously in many situations. The dominant damage mechanism will then depend on a particular material, its microstructure and external conditions (H concentration, type of loading, strain rate, temperature, etc.).

It has been shown by Bechtle et al. [7] that the fracture mode of polycrystalline Ni changes sharply from intragranular and ductile to intergranular and brittle when the material is charged with H. However, the transition depends sensitively on the Ni microstructure and the presence and fraction of special grain boundaries (GBs). These observations clearly indicate that hydrogen affects the cohesive strength of grain boundaries, as proposed in the HEDE mechanism, and that the sensitivity of a GB to HE likely depends on its interface structure [7, 8]. Nevertheless, in a follow-up work Martin et al. [9] concluded that plasticity always plays an important role in hydrogen-induced embrittlement in Ni, even when the macroscopic fracture appears to be brittle. The HELP mechanism, considering the variations of dislocation mobility due to hydrogen, can therefore be a contributing factor as well. In addition, a possible formation of a Ni nanohydride phase in the vicity of crack tips, dislocations and GBs has been proposed recently based on results of atomistic simulations [10, 11].

A key element common to all HE mechanisms is the need for a critical local concentration of hydrogen in the metal. In the case of the HEDE mechanism, this critical concentration needs to be achieved in the vicinity of the failing GBs at an accumulation rate comparable with the propagation rate of a crack [12, 13]. In order to fulfill this requirement, it is necessary for the H atoms to be both able to diffuse fast towards the GBs and become efficiently trapped there. Whereas most reports in the literature [14, 15, 16, 17, 18, 19] agree on favorable trapping properties of GBs, it is still rather controversial whether the GBs can also enhance H diffusion [3, 14, 16, 18, 20, 21, 22]. This controversy stems from a complicated interplay between intrinsic material properties, microstructure, and external conditions, but it is also partly due to a lack of systematic atomic-scale information regarding the diffusion of H along GBs. So far, only a few experimental studies [16, 23, 24] have considered, for example, the dependence of the H diffusivity at GBs on their interface character. Moreover, in experimental studies it is often difficult to exclude effects of other structural imperfections, such as point defects, dislocations, or impurities, which can all influence the diffusion measurements. In computational studies, the major difficulty lies in the massive amount of work required to identify and investigate representative cases from the vir-

tually infinite variety of possible GBs in materials.

In order to shed some light on this problem, we have investigated the trapping and diffusion of H across and along GBs in Ni using first-principles calculations. Two symmetric tilt grain boundaries (STGBs) have been selected for our study: the $\Sigma5(210)[001]$ STGB and the $\Sigma3(111)[\bar{1}10]$ STGB. These GBs (denoted briefly as $\Sigma5$ and $\Sigma3$ in the following) have very distinct interface structures and, as discussed in detail below, can be considered as representative cases for a broader variety of GB types.

The paper is organized as follows: In Sec. 2, we describe our computational approach. In Sec. 3, our results regarding the interface structures, the H segregation and the H diffusion for both GBs are presented. In Sec. 4, we discuss the results and provide a detailed comparison with available experimental and other theoretical results. In Sec. 5, the main findings and conclusions of the work are summarized.

2. Computational approach

Atomistic supercell models of the two GBs were investigated by means of density functional theory simulations using the Vienna ab-initio simulation package (VASP) [25, 26, 27]. A generalized gradient approximation (GGA) in the form given by Perdew, Burke and Ernzerhof [28] was employed for exchange-correlation and ultrasoft pseudopotentials [29] were used for the core-valence interactions. All calculations were carried out as spin-polarized. For the Brillouin-zone integrations, Monkhorst-Pack k-point meshes of 6x10x1 for the $\Sigma3$ and 4x8x2 for the $\Sigma5$ were used. For supercells without H, both ionic positions and cell vectors were relaxed. In supercells containing H atom, the dimensions were kept fixed (identical to the corresponding supercells without H) and only the ionic positions were relaxed.

The investigated GBs are characterized by the GB energy calculated as

$$\gamma_{GB} = \frac{E_{GB} - E_{bulk}}{2A}, \quad (1)$$

where E_{GB} is the total energy of the supercell containing the GB, E_{bulk} is the total energy of bulk Ni crystal with the same number of atoms, and A is the interface area of one GB in the supercell (the factor of two in the denominator takes into account that there are two identical GBs in the supercell). Lower values of γ_{GB} generally indicate a stronger cohesive bonding between the two grains in contact. Another useful parameter characterizing the GBs is the associated excess volume per one GB in the supercell defined as

$$\Delta V = \frac{V_{GB} - NV_{Ni}}{2}, \quad (2)$$

where V_{GB} is the total volume of the supercell containing the GB, N is the number of atoms in the supercell, and V_{Ni} is the volume per atom of bulk Ni. Larger values of ΔV indicate a more open GB structure, while smaller values indicate a more compact GB structure.

The efficiency of a GB to trap H atoms is quantified by the segregation energy, E^{seg}, defined as

$$E^{seg} = E^{sol}_{GB} - E^{sol}_{bulk}, \quad (3)$$

where the E^{sol}_{GB} and E^{sol}_{bulk} are the solution energies of H segregated at the GB and in the middle of the grain (in the same supercell), respectively. The solution energy for an H atom at a site x is defined as

$$E^{sol}_x = E_{x+H} - E_x - \frac{1}{2}E_{H_2}, \quad (4)$$

where E_{x+H} is the total energy of supercell containing H, E_x is the total energy of the same supercell without H, and E_{H_2} is the energy of an isolated H_2 molecule. With these definitions, negative values of the solution energies indicate that it is energetically more favorable for H to be dissociated and absorbed in Ni, while negative values of the segregation energies imply a preferable segregation of H at the GB.

3. Results

3.1. H in bulk Ni

As a reference, we first computed properties of bulk Ni in its face-centered cubic (fcc) equilibrium structure as well as H solution energies and migration barriers in a large bulk supercell containing 32 Ni atoms. The equilibrium lattice parameter of 3.53 Å for fcc Ni is in good agreement with other theoretical and experimental data [17, 11]. The calculated solution energy for H occupying an octahedral interstitial site in the large supercell amounts to 0.084 eV, similar to values obtained in other computational studies [11, 30, 31]. The migration of an H atom between two neighboring octahedral sites proceeds via an intermediate metastable tetrahedral site (see Fig. 4(a)). The calculated energy barrier associated with the jump was found to be 0.37 eV without mechanical effects [32, 33]. This result closely agrees with results of previous calculations [34, 35]. We investigated in detail the influence of quantum corrections [2, 32, 34, 35, 36] using the semi-classically corrected transition state theory [37, 38] and found that these corrections are relatively small for Ni and do not affect the results presented here. This investigation will be reported elsewhere [39].

Structure of the $\Sigma3(111)[\bar{1}10]$ *GB*

The $\Sigma3$ GB supercell consists of an orthorhombic cell with 24 Ni atoms and contains two GBs separated by five atomic (111) layers. The relaxed GB structure is shown in Fig. 1, the corresponding supercell dimensions and the GB energy are given in Table 1. The first-nearest-neighbor distances between Ni atoms in the vicinity of the GB deviate less than a half percent from the bulk value of 2.50 Å indicating that the atomic arrangement at the interface

is only slightly distorted. This is not surprising, since the presence of this twin interface only alters the stacking of the close-packed (111) planes. As a result, the Σ3 GB has a negligible excess volume (see Table 1), and the calculated GB energy of 0.18 J/m^2 is very small in comparison with typical GB energies values [40].

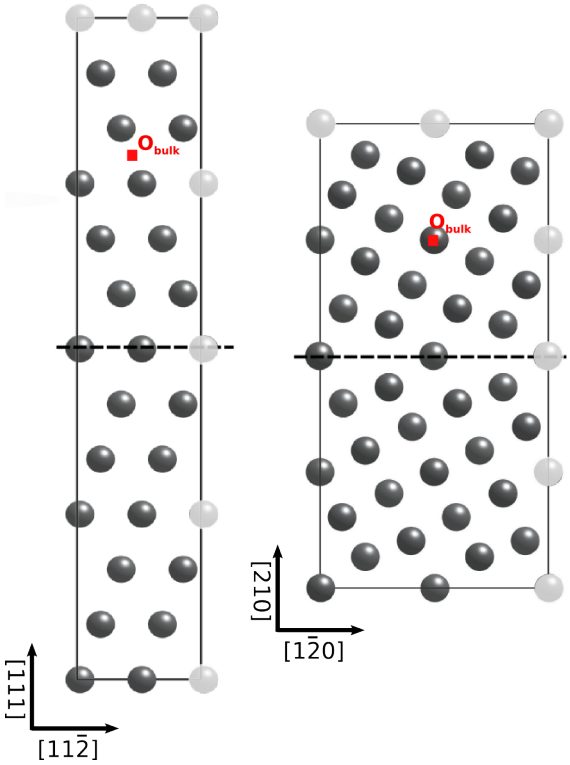


Figure 1: Relaxed supercells for the Σ3 GB (left) and for the Σ5 GB (right) containing 24 and 40 Ni atoms, respectively. The dashed lines mark the GB interface planes; the repeated atoms are shown in light grey; the bulk octahedral sites are marked by red squares.

STGB	a [Å]	b [Å]	c [Å]	γ_{GB} [J/m^2]	ΔV [Å^3]
Σ3(111)[$\bar{1}$10]	4.320	2.502	24.51	0.18	0.8
Σ5(210)[001]	7.928	3.545	16.41	1.29	11.1

Table 1: Supercell dimensions, GB energies, γ_{GB}, and excess volumes per one GB, ΔV, for the relaxed supercells of the two investigated GBs.

Structure of the Σ5(210)[001] *GB*

The orthorhombic supercell of the Σ5 GB contains 40 Ni atoms distributed on 10 atomic (210) layers. Previous studies [15, 17, 41] have shown that this supercell is sufficiently large to avoid spurious interactions between two GBs. The relaxed GB structure is shown in Fig. 1, additional characteristic data are listed in Table 1.

In contrast to the Σ3 GB, the local atomic and electronic structure of the Σ5 GB is significantly different with respect to the bulk interior. In order to visualize these differences, we plot several cross sections showing the valence electron densities in the Σ5 supercell in Fig. 2. In the central (bulk) part of the supercell (see the cross section in Fig. 2b), the regions of the lowest electron density are located at the ordinary octahedral interstitial sites in bulk Ni. In contrast, much larger regions of low electron density are present along the GB plane (see Fig. 2a and 2c). We refer to these regions further as cavities and analyze their role in H segregation and diffusion in detail below. The presence of the cavities along the GB plane reflects the more open structure of the Σ5 GB, characterized by much larger excess volume than that for the Σ3 GB (cf. Table 1). In addition, the distorted atomic structure also leads to a significantly higher GB energy, comparable to energies of most GBs in Ni [40].

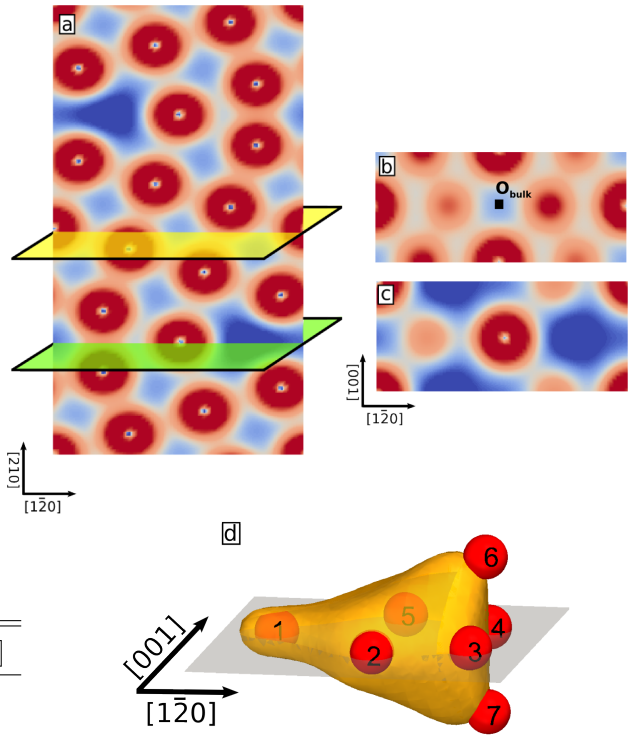


Figure 2: (Color online) Valence electron density plots for the Σ5 GB: panel (a) shows a cross section along the (001) plane, panels (b) and (c) depict cross sections along two (210) planes in the bulk-like region (highlighted in yellow in (a)) and at the GB plane (highlighted in green in (a)). The red and blue colors correspond to areas of high and low electron densities, respectively. The region of the lowest electron density in the bulk cross section corresponds to an ordinary octahedral site. On the (a) and (c) cross sections, the GB cavities with low electron density are clearly visible in blue. (d) A 3D depiction of the GB cavity as an isosurface corresponding to electron density of 0.14 Å^{-1}); the superimposed red spheres mark the metastable segregation sites for hydrogen atoms.

H segregation at the GBs

In order to quantify H segregation, an H atom was inserted at various interstitial positions in the two GB supercells, and the structures were subsequently relaxed. For

the Σ3 GB, two sites were selected: (i) a bulk-like octahedral site in the middle of the supercell (further referred to as $O^{\Sigma3}_{bulk}$ site), and (ii) an octahedral site located in between the GB plane and its immediately neighboring (111) plane (further referred to as $O^{\Sigma3}_{GB}$ site). The reason why the H atom was not placed directly at the GB plane is that due to the local A-B-A stacking of the (111) planes, there are no octahedral interstitial sites at the GB plane (see Fig. 4b and discussion below). The segregation and solution energies, calculated according to Eqs. 3 and 4, are listed in Table 2.

The solution energy of 0.08 eV in the bulk region of the GB supercell is the same as the value for the reference bulk configuration mentioned above. In case of the $O^{\Sigma3}_{GB}$ site, the solution and segregation energies are only marginally lower than those in the bulk. The small segregation energy of only −0.01 eV indicates that the trapping of H at the Σ3 GB is almost negligible.

Site	E^{sol}_x [eV]	E^{seg} [eV]	ρ_{el} [Å^{-3}]
$O^{\Sigma3}_{bulk}$	0.08	0.00	0.18
$O^{\Sigma3}_{GB}$	0.07	−0.01	0.18
$O^{\Sigma5}_{bulk}$	0.09	0.00	0.18
$O^{\Sigma5}_{GB+1}$	0.10	0.01	0.18
$T^{\Sigma5}_{GB}$	0.06	0.03	0.23
$S^{\Sigma5}_1$	-0.14	−0.23	0.13
$S^{\Sigma5}_2$,$S^{\Sigma5}_5$	−0.13	−0.22	0.13
$S^{\Sigma5}_3$,$S^{\Sigma5}_4$	0.00	−0.09	0.15
$S^{\Sigma5}_6$,$S^{\Sigma5}_7$	−0.08	−0.17	0.15

Table 2: Solution and segregation energies for various bulk-like (marked with subscript *bulk*) and interface (marked with subscript *GB*) sites in the two investigated GB supercells. The *O* labels correspond to sites with the octahedral symmetry, the *S* and *T* labels correspond to the metastable sites within the Σ5 GB shown in Figs. 3(a) and 5.

In the case of the Σ5 GB, the number and variability of possible segregation sites is much larger. For the bulk octahedral site (further referred to as $O^{\Sigma5}_{bulk}$) in the middle of a grain (see Figs. 1 and 2), we again obtain the solution energy that is very similiar to the reference solution energy for H in bulk Ni. Within the GB cavity, we were able to identify seven metastable sites (further referred to as $S^{\Sigma5}_1$ to $S^{\Sigma5}_7$) where H can segregate, as illustrated in Fig. 2d. Most of the sites ($S^{\Sigma5}_1$ to $S^{\Sigma5}_5$) lie on the GB plane, while the sites $S^{\Sigma5}_6$ and $S^{\Sigma5}_7$ are located approximately at the level of the (210) Ni planes adjacent to the GB plane. Due to the mirror symmetry of the GB cavity with respect to the (001) and (210) planes, the sites 2 and 5, 3 and 4, and 6 and 7 are equivalent. For all these sites, the computed segregation energies are negative (cf. Table 2), but the values for the most and least trapping site differ by more

(a)

(b)

Figure 3: (Color online) Segregation energies for metastable H sites (full symbols) and associated transition states (empty symbols) for H migration across (a) and along (b) the Σ5 GB. The full and dashed lines correspond to relaxed and unrelaxed NEB calculations, respectively. The black symbols connected by the dotted black line represent the minimum energy path for H migration in bulk Ni.

than 0.1 eV. In addition, we also explored several interstitial sites surrounding the GB cavity and identified two sites, one with tetrahedral ($T^{\Sigma5}_{GB}$) and one with octahedral ($O^{\Sigma5}_{GB+1}$) symmetries, that are most relevant for the H migration to/from the GB cavity (see Fig. 4c and discussion in the next section).

In order to relate the calculated segregation energies to the underlying electronic structure of the GBs, we also analyzed the electron density, ρ_{el}, at all sites before inserting the H atom. The obtained values are listed in the last column of Table 2. The reference electron densities at octahedral and tetrahedral sites in the bulk Ni supercell amounting to 0.18 and 0.25 Å^{-3}, respectively, are fully consistent with the values found in the GB supercells. In contrast, the electron densities at the most favorable segregation sites within the Σ5 cavity are significantly smaller. The lowest electron density of only 0.07 Å^{-3} was found in the middle of the GB cavity.

H migration to, across and along the GBs

The distorted atomic structure of GBs is expected to alter also the local migration pathways and associated energy barriers for H jumps. We investigated the H migration in the vicinity of both GBs using either the NEB method or, in a few cases, just a linear interpolation between the initial and final states without relaxing the intermediate atomic configurations (i.e., effectively unrelaxed NEB calculations).

In the case of the Σ3 GB, we used NEB to calculate the minimum energy paths (MEPs) for H jumps in three distinct cases: (i) a jump between two bulk-like octahedral sites remote from the GB, (ii) a jump between two neighboring octahedral sites parallel to the GB, and (iii) a jump between two octahedral sites across the GB plane. It turned out that in the first two cases the MEP is equal to that in the perfect crystal, where the migration takes place through a metastable tetrahedral site (see Fig. 4a), with a calculated migration energy barrier of 0.37 eV. In the third case, the migration path differs from the bulk case since the neighboring octahedra across the GB plane share their faces instead of edges as in bulk (compare panels a and b of Fig. 4). As a result, the neighboring octahedral sites across the GB plane are connected without the intermediate tetrahedral site. This path is characterized by a calculated migration energy barrier of 0.55 eV, which is

almost 50% higher than the barrier in bulk Ni. This indicates that the Σ3 GB acts as a two-dimensional barrier for H diffusion.

In the case of the Σ5 GB, the migration pathways are much more complex and we therefore analyzed separately the H jumps along and across the GB. For H migration along the GB plane, we employed the NEB method to calculate the minimum energy paths connecting the sites $S_1^{\Sigma5}$ to $S_5^{\Sigma5}$, both within a single cavity and between neighboring cavities. The results of these NEB calculations were interpolated to obtain the whole potential energy surface (PES) for H migration along the Σ5 GB plane (see Fig. 5). The migration barriers for the most relevant transition states are shown in Fig. 3b. The five locally stable positions inside the cavity are connected by saddle points of relatively low migration barriers, not exceeding 0.22 eV, so that H can move rather freely inside the cavity. Transitions between neighboring cavities can occur via two distinct paths, namely, between sites $S_1^{\Sigma5}$ and $S_{3'}^{\Sigma5}$ or $S_5^{\Sigma5}$ and $S_{2'}^{\Sigma5}$ (see Fig. 5). These transitions are characterized by migration barriers which are somewhat higher than those inside the cavities but still significantly lower than the barrier of 0.37 eV between two octahedral sites in bulk Ni. The highest barrier within the GB corresponds to the jump from $S_1^{\Sigma5}$ to $S_{3'}^{\Sigma5}$ with an energy of 0.27 eV. This energy barrier can be therefore considered as the determining barrier for the diffusion of H atoms along the GB plane. Furthermore, since the migration barrier for the $S_5^{\Sigma5}$ to $S_{2'}^{\Sigma5}$ and $S_2^{\Sigma5}$ to $S_3^{\Sigma5}$ are only marginally lower (0.24 and 0.22 eV), the diffusion within the Σ5 GB plane can be considered as isotropic.

For H diffusion across the Σ5 GB, the crucial events are jumps to/from the most favorable segregation sites inside the GB cavity. We identified a MEP joining the $S_6^{\Sigma5}$ site via the adjacent tetrahedral site $T_{GB}^{\Sigma5}$ to a bulk-like octahedral site $O_{GB+1}^{\Sigma5}$. The local atomic configurations around these sites are displayed in Fig. 4c. In addition, we also investigated the transitions between the cavity sites lying directly on the GB plane (i.e., $S_1^{\Sigma5}$ to $S_5^{\Sigma5}$) and the $S_6^{\Sigma5}$ and $S_7^{\Sigma5}$ sites located in two cavity lobes extending away from the GB plane (cf. Fig 2c). Due to high computational costs, only the $S_6^{\Sigma5}$ to $T_{GB}^{\Sigma5}$ jump was calculated using NEB. The remaining barriers (marked by dashed lines in Fig. 3a) were obtained from linear interpolations between the metastable configurations without relaxing the NEB. They therefore correspond to upper limits of the barriers. The results in Fig. 3a show that the barriers for H migration from bulk towards the GB plane are very low. The rate-controlling event for H to escape from the GB is the jump from the cavity to the $T_{GB}^{\Sigma5}$ site with migration energy of 0.27 eV. This barrier is higher than those for H migration along the GB plane, but it is still significantly lower than the barrier for H diffusion inside bulk Ni.

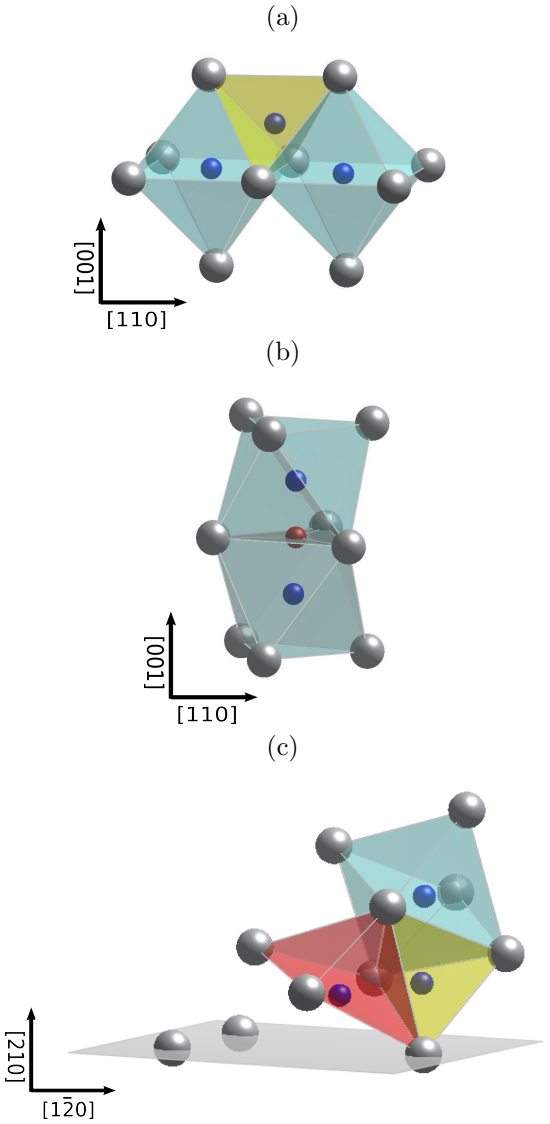


Figure 4: (Color online) (a) Atomic arrangement of bulk fcc Ni showing two octahedra connected by their edges. The MEP for H diffusing between the neighboring octahedral interstitial sites (blue spheres) goes via the metastable tetrahedral position (black sphere in the center of the yellow tetrahedron). (b) In the Σ3 GB, the octahedra share their faces parallel to the GB plane with a saddle-point position (red sphere) in the center of the shared triangle. (c) Local atomic structure around the $S_6^{\Sigma5}$ (blue sphere in red pyramid, tetrahedral site $T_{GB}^{\Sigma5}$ (blue sphere in the yellow tetrahedron), and octahedral site $O_{GB+1}^{\Sigma5}$ (blue sphere in the blue octahedron) relevant for the migration to/from the Σ5 GB.

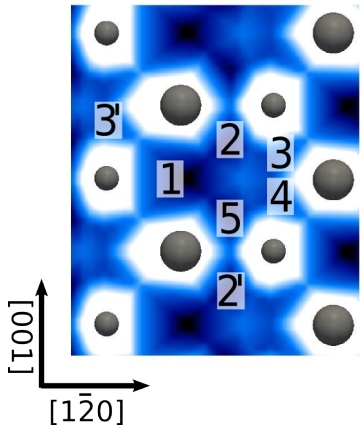


Figure 5: (Color online) Potential energy surface for H along the Σ5 GB plane obtained by interpolation of several NEB calculations. Dark blue and black colors indicate the energy minima, light blue colors indicate regions of intermediate energies, and the white color corresponds to high-energy regions of H repulsion very close to Ni atoms (grey balls) that have not been sampled. The labels $1-5$ correspond to the metastable positions, $S_x^{\Sigma5}$, listed in Table 2; note that the sites 3, 4 and 3', as well as 2, 5 and 2', are equivalent.

4. Discussion

In the present work, we investigate the interaction between atomic H and two GBs in Ni with distinct local atomic structures. The Σ3(111)[$\bar{1}$10] STGB is the most perfect GB in fcc crystals, and its coherent atomic structure composed of close-packed (111) atomic layers results in a very low GB energy. In contrast, the Σ5(210)[001] STGB has a significantly distorted interface structure, with an open atomic arrangement characterized by rather large cavities at the GB plane. Consequently, its GB energy is rather high.

The different interfacial structures of the two considered GBs result in different interaction behaviors with H atoms. The first difference is with regard to H segregation. While the segregation energy for the Σ3 GB is negligibly small, the Σ5 GB possesses multiple trapping sites with moderate segregation energies ranging from -0.09 to -0.23 eV. This indicates that the Σ3 does not attract H atoms, whereas the Σ5 acts as an efficient two-dimensional sink for H. These results agree with those of previous computational studies on polycrystalline Ni. Geng et al. [15] and Yamaguchi et al. [17] have investigated the H segregation at the Σ5 GB and reported segregation energies of about the same value for the most stable site. It is also interesting to note that the segregation energy found for the interstitial H atoms at the cavity of the Σ5 GB agrees surprising well with the value of -0.27 eV reported by other investigators [30, 31] for H trapped at a vacancy in bulk Ni. This result may be surprising at first, since it does not correlate with the excess volume, which is about twice as large for the vacancy ($V_{vac} = 11.0$ Å^3) than for the GB cavity ($V_{cav} = 5.5$ Å^3). However, it becomes clear when taking into consideration that the most stable H sites in both cases are not at the locations of the lowest electron density, but instead H atoms prefer to attach to internal surfaces of the two defects where the electron density is higher. The existence of an optimum electron density for H binding (chemisorption) to a metal has been predicted within the effective medium theory (EMT) [42, 43, 1]. Our calculations confirm the correlation between the electon density and the segregation energy (cf. Table 2) with the optimum electron density ranging between 0.13-0.15 Å^{-3} at the internal surfaces of the GB cavity. For electron densities higher than 0.15 Å^{-3} (e.g., in the bulk interstitial sites or transition states) or lower than 0.13 Å^{-3} (e.g., in the middle of a vacancy or the GB cavity) the segregation energies become smaller.

The second difference between the two investigated GBs concerns the diffusion of H. The migration of an H atom in the vicinity of the Σ3 GB parallel to the GB plane is essentially equal to its migration in the bulk interior of Ni. However, the diffusion across the GB plane is associated with a significantly higher barrier of 0.55 eV, compared to 0.37 eV in the bulk. Hence, this GB acts as a two-dimensional barrier for diffusing H atoms.

In contrast, the migration of H towards the Σ5 GB is characterized by energy barriers that are much lower than the bulk barrier. The diffusing H atoms can easily reach the favorable segregation sites inside the GB cavities, but the escape rates are much lower due to significantly higher migration barriers for the reverse jumps (cf. Fig. 3a). As a result, the Σ5 GB can also behave as a barrier for H diffusion, not because of higher migration barriers but due to effective trapping.

Since the migration along the Σ5 GB (i.e., within and between the cavities) is characterized by a mean migration barrier which is lower than that in the bulk by almost 30%, the diffusion along the GB is much faster than the bulk diffusion. To estimate the enhancement of the H diffusion along the Σ5 GB, we consider that the diffusion coefficient, D, is proportional to the jump rate, $\Gamma \propto e^{-\frac{\Delta E_{mig}}{kT}}$, and we assume similar prefactors for the diffusivities in the bulk and at the GB. We can then estimate the ratio between GB and bulk diffusivities at room temperature as

$$\frac{D_{\Sigma5}}{D_{bulk}} \sim e^{-\frac{\Delta E_{mig}^{\Sigma5} - \Delta E_{mig}^{bulk}}{kT}} \sim 10^2. \qquad (5)$$

This estimated value suggests that the H diffusivity at the atomic scale along the Σ5 GB is about two orders of magnitude greater than that in the perfect single crystal. For a more accurate treatment, it would be necessary to employ mesoscopic approaches, such as kinetic Monte Carlo simulations, to capture the influence of H trapping and concentration [19, 31]. Furthermore, it is important to bear in mind that the results obtained here are strictly valid just for local H migration around the GBs at the atomic scale. To describe properly the macroscopic diffusion of H in polycrystalline materials, it is necessary to calculate an effective diffusivity that depends strongly on

microstructural aspects such as grain size, distribution of GB types, and GB connectivity [44, 45, 46, 47, 48].

As mentioned above, the two investigated GBs have markedly different atomic structures and, consequently, exhibit very different interactions with H atoms. Nevertheless, we believe that the specific properties of these two GBs are applicable to and characteristic for a wider variety of GBs. In the following, we provide further support for this assumption by analyzing and comparing results of previous theoretical and experimental studies.

In polycrystalline materials, there are many grain misorientations and interface inclinations leading to a variety of GB types [49]. In this study, we did not consider low-angle GBs, which can be well described by dislocation networks, but we focused only on high-angle GBs with characteristic atomic structures. This class of GB can be divided into two subsets, namely, singular (often also called special) and general GBs [49]. In singular GBs, most of the interfacial atoms fit very well with both adjoining crystal structures and attain also a favorable configuration at the interface (e.g., metals favor dense packing of atoms). Because of the weak distortions and a favorable atomic structure, these GBs are at a local minimum in the energy with respect to geometrical degrees of freedom. On the contrary, in general GBs the atomic structure is strongly distorted and contains large regions of poor structural match of interfacial atoms and/or significant excess volumes. As a result of the distorted and more open structure, general GBs have higher interface energies than singular GBs.

Both GBs investigated in this work are singular GBs, but while the $\Sigma3$ twin boundary can be considered as the most coherent GB, the $\Sigma5$ has features that are more akin to a general GB, i.e., a more open structure composed of characteristic structural units (cf. Fig. 2), and a rather high GB energy (cf. Table 1). The results obtained for the $\Sigma5$ GB may be therefore considered as representative for general GBs as well. In order to validate this hypothesis, we performed a detailed comparison of experimental and other computational results, not only for Ni but also for other metals.

The comparison with experimental results is not easy because in most studies an effective diffusion in polycrystals is reported only. Because of that, we focus first on the recent studies of Oudriss et al. [16, 24], who carried out a systematic investigation of diffusion coefficients and migration energies for H in various Ni microstructures. The reported migration energy of 0.25 eV for general GBs is quantitatively consistent with the range of values obtained in our study for the H migration along the $\Sigma5$ GB. Even though it is not possible to identify the exact GB types from the reported experimental studies, this agreement gives weight to our hypothesis that $\Sigma5$ GB can be cautiously considered as a representative for general GBs. In addition, Oudriss et al. [16, 24] reported that the effective H diffusivity gradually increases by up to two orders of magnitude when the grain size is reduced, but for nanocrystalline Ni with grain diameters below 0.1 μm it decreases again. This enhancement of diffusivity with increasing fraction of GBs is again consistent with our results. However, the comparison is in this case not trivial due to additional effects of H concentration, trap filling, GB connectivity, and the presence of other crystal defects such as dislocations, which all likely affect the measured diffusivities. Also earlier experimental studies [23, 50, 51] consistently report an accelerated H diffusion with GB diffusivities being 1-2 orders of magnitude faster than the bulk diffusivity. Nevertheless, as already pointed out, it is difficult to make quantitative comparisons.

A very limited number of atomistic simulation studies on H diffusion at Ni GBs are available in the literature. Molecular dynamics studies [21, 52] based on an embedded-atom method potential of Angelo and Baskes [53] showed a significant enhancement of H diffusion at various Ni GBs. To our knowledge, no first-principles calculations exist for Ni, but Du et al. [14] investigated recently the interaction of H with GBs in fcc Fe using DFT. Similar to our study, they considered two different GB types – $\Sigma3(111)[1\bar{1}0]$ and $\Sigma11(113)[1\bar{1}0]$ STGBs, as representatives of dense and open GB structures. In neither of these two GBs H trapping or diffusion enhancement was found. While these results are consistent with ours for the $\Sigma3$ GB, they appear contradictory for the open $\Sigma11$ GB, which would be expected to behave similarly to our open $\Sigma5$ GB. However, the $\Sigma11(113)[1\bar{1}0]$ is known to be an atypical GB with not only a very low GB energy but also very small excess volume [49, 54, 40]. This GB is therefore more akin to the $\Sigma3$ than to the $\Sigma5$ GB.

In another study, Pedersen et al. [18] used an EMT potential fitted to DFT data to investigate the H interaction with different GBs in Al. According to their kinetic Monte Carlo simulations, none of the inspected GBs showed an enhanced H diffusivity. Even though these results have to be taken with caution due to the empirical nature of the EMT potential, this result may be related to a faster H diffusion in bulk Al. Because Al has a larger lattice parameter than Ni, H prefers to occupy tetrahedral interstitial sites in Al, and the migration barrier for H in Al is only half of that in Ni [55]. The migration energies within the GB plane reported by Pedersen et al. [18] are similar to our values for the $\Sigma5$ GB, but due to faster bulk diffusion the H diffusivities at the GBs are not enhanced but rather impeded.

This outcome may be common to other fcc metals with high bulk diffusivities as well as to bcc metals, where the H diffusion is generally very fast. In order to corroborate this hypothesis, additional investigations are necessary, but a partial confirmation can be given considering the cases of fcc Pd and bcc Fe. Pd has a low bulk migration energy of about 0.2 eV [2], and GBs were found to impede H diffusion [56] as in the case of Al. H in bcc Fe has a very low energy barrier for bulk migration, and also in this case no diffusion enhancement was observed [20].

5. Summary and conclusions

First-principles calculations based on density functional theory have been performed to investigate different aspects of H atoms interacting with grain boundaries in Ni. Two model GBs, $\Sigma3(111)[\bar{1}10]$ and $\Sigma5(210)[001]$, have been selected and their interface atomic and electronic structures carefully analyzed. Both the segregation of H at various interstitial sites in the vicinity of the GBs and the migration of H towards and along the GBs have been studied in detail. The key results of our study are:

1. The H trapping and migration depend strongly on the GB character.
2. The $\Sigma3$ STGB does not trap H atoms and acts as a two-dimensional obstacle for H diffusion.
3. The $\Sigma5$ STGB acts as an effective two-dimensional sink for H atoms, but provides fast migration channels along the GB plane where H can diffuse about two orders of magnitude faster than in bulk Ni.

Our results are consistent with those of other computational and experimental studies. Based on comparisons with available literature data, we presume that the chosen GBs can be considered as representatives for a larger variety of GB types. The results obtained for Ni can be also transfered to other metals, but it is always necesary to consider the GB effects with respect to bulk diffusion. If the bulk diffusion is sufficiently fast, the effect of enhanced diffusion along GBs can be negligible, or the trapping may even prevail.

We believe that our results help to clarify some apparent controversies in the literature about the effect of GBs on diffusion of H. Nonetheless, an ultimate answer to that issue requires further investigations, by experiment and simulation, of the H diffusion in properly designed polycrystalline microstructures with well defined GBs.

6. Acknowledgments

This work was supported by the European Union within the Seventh Framework Programme, grant number 263335, MultiHy (Multiscale Modeling of Hydrogen Embrittlement in Crystalline Materials).

References

[1] S. M. Myers, M. Baskes, H. Birnbaum, J. W. Corbett, G. G. DeLeo, S. K. Estreicher, E. Haller, P. Jena, N. M. Johnson, R. Kirchheim, S. Pearton, M. Stavola, Rev. Mod. Phys. 64 (1992) 559.
[2] Y. Fukai, The Metal-Hydrogen System, Springer, 2004.
[3] A. Pundt, R. Kirchheim, Annu. Rev. Mater. Res. 36 (2006) 555.
[4] I. Robertson, H. Birnbaum, P. Sofronis, Dislocations in Solids 15 (2009) 249.
[5] S. Lynch, Corros. Rev. 30 (2012) 2969.
[6] I. M. Robertson, P. Sofronis, A. Nagao, M. L. Martin, S. Wang, D. W. Gross, K. E. Nygren, Metall. Mater. Trans. A 46 (2015) 2323.
[7] S. Bechtle, M. Kumar, B. Somerday, M. Launey, R. Ritchie, Acta Mater. 57 (2009) 4148.
[8] M. Seita, J. P. Hanson, S. Gradečak, M. J. Demkowicz, Nat. Commun. 6 (2015) 6164.
[9] M. L. Martin, B. P. Somerday, R. O. Ritchie, P. Sofronis, I. M. Robertson, Acta Mater. 60 (2012) 2739.
[10] J. Song, W. Curtin, Acta Mater. 59 (2011) 1557.
[11] J. von Pezold, L. Lymperakis, J. Neugebauer, Acta Mater. 59 (2011) 2969.
[12] S. Wang, M. L. Martin, P. Sofronis, S. Ohnuki, N. Hashimoto, I. M. Robertson, Acta Mater. 69 (2014) 275.
[13] M. Dadfarnia, P. Novak, D. C. Ahn, J. B. Liu, P. Sofronis, D. D. Johnson, I. M. Robertson, Adv. Mater. 22 (2010) 1128.
[14] Y. A. Du, L. Ismer, J. Rogal, T. Hickel, J. Neugebauer, R. Drautz, Phys. Rev. B 84 (2011) 144121.
[15] W. Geng, A. Freeman, R. Wu, C. Geller, J. Raynolds, Phys. Rev. B 60 (1999) 7149.
[16] A. Oudriss, J. Creus, J. Bouhattate, E. Conforto, C. Berziou, C. Savall, X. Feaugas, Acta Mater. 60 (2012) 6814.
[17] M. Yamaguchi, M. Shiga, H. Kaburaki, J. Phys. Soc. Jpn. 73 (1990) 441.
[18] A. Pedersen, H. Jònsson, Acta Mater. 57 (2009) 4036.
[19] X. J. Shen, D. Tanguy, D. Connétable, Philos. Mag. 94 (2014) 2247.
[20] Y. A. Du, J. Rogal, R. Drautz, Phys. Rev. B 86 (2012) 174110.
[21] B. Szpunar, L. J. Lewis, I. Swainson, U. Erb, Phys. Rev. B 60 (1999) 10107.
[22] K. Ichitani, M. Kanno, Sci. Technol. Adv. Mater. 4 (2003) 545.
[23] B. Ladna, H. K. Birnbaum, Acta Metall. 35 (1987) 2537.
[24] A. Oudriss, J. Creus, J. Bouhattate, C. Savall, B. Peraudeau, X. Feaugas, Scripta Mater. 66 (2012) 37.
[25] G. Kresse, J. Hafner, Phys. Rev. B 48 (1993) 13115.
[26] G. Kresse, J. Furthmueller, Phys. Rev. B 54 (1996) 11169.
[27] G. Kresse, J. Furthmueller, Comput. Mater. Sci. 6 (1996) 15.
[28] J. Perdew, K. Burke, M. Ernzerhof, Phys. Rev. Lett. 77 (1996) 3865.
[29] D. Vanderbilt, Phys. Rev. B 41 (1990) 7892.
[30] D. Connétable, Y. Wang, D. Tanguy, J. Alloys Comp. 614 (2014) 211.
[31] D. Tanguy, Y. Wang, D. Connétable, Acta Mater. 78 (2014) 135.
[32] I. H. Katzarov, D. L. Pashov, A. T. Paxton, Phys. Rev. B 88 (2013) 054107.
[33] T. Yoshikawa, T. Takayanagi, H. Kimizuka, M. Shiga, J. Phys. Chem. 116 (2012) 23113.
[34] C. Elsässer, H. Krimmel, M. Fähnle, S. G. Louie, C. T. Chan, J. Phys. Condens. Matter 10 (1998) 5131.
[35] E. Wimmer, W. Wolf, J. Sticht, P. Saxe, C. B. Geller, R. Najafabadi, G. A. Young, Phys. Rev. B 77 (2008) 134305.
[36] H. Kimizuka, H. Mori, S. Ogata, Phys. Rev. B 83 (2011) 094110.
[37] B. Bhatia, D. S. Sholl, Phys. Rev. B 72 (2005) 224302.
[38] D. S. Sholl, J. Alloys Comp. 446 (2007) 462.
[39] D. Di Stefano, M. Mrovec, C. Elsässer, 2015. In preparation.
[40] D. L. Olmsted, S. M. Foiles, E. A. Holm, Acta Mater. 57 (2009) 3694.
[41] M. Všianská, M. Šob, Prog. Mater. Sci. 56 (2011) 817.
[42] J. Nørskov, Phys. Rev. B 26 (1982) 2875.
[43] P. Nordlander, J. Nørskov, F. Besenbacher, J. Phys. F: Met. Phys. 16 (1986) 1161.
[44] E. Legrand, J. Bouhattate, X. Feaugas, S. Touzain, H. Garmestani, M. Khaleel, D. Li, Comp. Mater. Sci. 71 (2013) 1.
[45] S. Jothi, T. Croft, S. Brown, Int. J. Hydrogen Energy 39 (2014) 20671.
[46] B. Osman Hoch, A. Metsue, J. Bouhattate, X. Feaugas, Comput. Mater. Sci. 97 (2015) 276.
[47] S. Jothi, N. Winzer, T. Croft, S. Brown, J. Alloys Comp. In press (2015).
[48] E. Reese, W. Von Bestenbostel, T. Sebald, G. Paronis, D. Vanelli, Y. Müller, JOM 66 (2014) 1368.
[49] A. P. Sutton, R. W. Balluffi, Interfaces in Crystalline Materials, Clarendon Press, Oxford, 1995.

[50] D. R. Arantes, X. Y. Huang, C. Marte, R. Kirchheim, Acta Metal. Mater. 41 (1993) 3215.
[51] A. M. Brass, A. Chanfreau, Acta Mater. 44 (1996) 3823.
[52] J. Skogsrud, C. Thaulow, 2014. Unpublished.
[53] J. E. Angelo, N. R. Moody, M. I. Baskes, Modelling Simul. Mater. Sci. Eng. 3 (1995) 289.
[54] G. Hasson, J. Y. Boos, I. Herbeuval, M. Biscondi, C. Goux, Surf. Sci. 31 (1972) 115.
[55] C. Wolverton, V. Ozolinš, M. Asta, Phys. Rev. B 69 (2004) 144109.
[56] T. Mütschelle, R. Kirchheim, Scripta Metall. 14 (1987) 1101.